

# The evolutionary inheritance of elemental stoichiometry in marine phytoplankton

Antonietta Quigg<sup>1</sup>, Zoe V. Finkel<sup>1</sup>, Andrew J. Irwin<sup>1</sup>, Yair Rosenthal<sup>1,2</sup>, Tung-Yuan Ho<sup>5</sup>, John R. Reinfelder<sup>3</sup>, Oscar Schofield<sup>1,4</sup>, Francois M. M. Morel<sup>5</sup> & Paul G. Falkowski<sup>1,2</sup>

<sup>1</sup>Environmental Biophysics and Molecular Ecology Program, Institute of Marine and Coastal Sciences, <sup>2</sup>Department of Geological Sciences, <sup>3</sup>Department of Environmental Sciences, and <sup>4</sup>Coastal Ocean Observation Laboratory, Rutgers University, New Jersey 08901, USA

<sup>5</sup>Department of Geosciences, Princeton University, New Jersey 08544, USA

Phytoplankton is a nineteenth century ecological construct for a biologically diverse group of pelagic photoautotrophs that share common metabolic functions but not evolutionary histories<sup>1</sup>. In contrast to terrestrial plants, a major schism occurred in the evolution of the eukaryotic phytoplankton that gave rise to two major plastid superfamilies<sup>2–4</sup>. The green superfamily appropriated chlorophyll *b*, whereas the red superfamily uses chlorophyll *c* as an accessory photosynthetic pigment<sup>5</sup>. Fossil evidence suggests that the green superfamily dominated Palaeozoic oceans. However, after the end-Permian extinction, members of the red superfamily rose to ecological prominence. The processes responsible for this shift are obscure. Here we present an analysis of major nutrients and trace elements in 15 species of marine phytoplankton from the two superfamilies. Our results indicate that there are systematic phylogenetic differences in the two plastid types where macronutrient (carbon:nitrogen:phosphorus) stoichiometries primarily reflect ancestral pre-symbiotic host cell phenotypes, but trace element composition reflects differences in the acquired plastids. The compositional differences between the two plastid superfamilies suggest that changes in ocean redox state strongly influenced the evolution and selection of eukaryotic phytoplankton since the Proterozoic era.

To examine patterns of variation in biochemical composition, 15 species of marine eukaryotic phytoplankton from five phyla were grown using axenic techniques under identical conditions ( $19 \pm 1^\circ\text{C}$ ; 12 h light/dark cycle;  $250 \mu\text{mol photons m}^{-2} \text{s}^{-1}$ ). The average bulk elemental composition of  $\text{C}_{125}:\text{N}_{16}:\text{P}_1$ , by atoms, for the ensemble of phytoplankton (see Supplementary Fig. 1) was remarkably similar to the canonical stoichiometry ( $\text{C}_{106}:\text{N}_{16}:\text{P}_1$ ) first recognized by Redfield<sup>6</sup> as early as 1934 to have a causal correlation with the  $\text{NO}_3^-$  and  $\text{PO}_4^{3-}$  ratio in the ocean interior. The basic concept of the Redfield ratio became a cornerstone of ocean models in the ensuing decades; it represents an emergent property that integrates biogeochemical cycles on basin scales over tens of thousands of years<sup>7</sup>. It was clearly understood however, that “The ratios hold very well for the nitrate and phosphate in ocean waters, but, since they represent the net effect of biological activity, marked deviations from the ratios may be found in individual types of organisms”<sup>8</sup>.

Indeed, there are systematic variations in C:N:P ratios between different eukaryotic phyla and superfamilies. The differences in C:P and C:N ratios between phyla and superfamilies (Fig. 1) are statistically significant ( $P < 0.01$ ; see Supplementary Table 1). Whereas N:P ratios differentiate between the superfamilies ( $P < 0.01$ ), this was not the case for phyla (Fig. 1). Experimental evidence suggests that differences in cellular N:P composition between marine eukaryotic phytoplankton is a reflection of the ratio of total cell protein to ribosomal RNA<sup>9–11</sup>, but not genome size. That we can differentiate between phyla and superfamilies supports

the suggestion that the C:N:P composition of particulate organic matter is dependent on the species composition of a phytoplankton assemblage. Hence, given the species composition of a phytoplankton assemblage, one could predict with reasonable precision the average C:N:P ratio of the ensemble community, but not vice versa.

By extending the compositional analysis to include the trace elements Fe, Mn, Zn, Cu, Cd, Co and Mo (see Supplementary Fig. 1), we were able to further differentiate between eukaryotic marine phytoplankton phyla (see Supplementary Table 1) and superfamilies ( $P < 0.001$ ; analysis of variance (ANOVA)). To define stoichiometric elemental profiles, we considered the trace elemental data in aggregate using principal component analysis (PCA). The first two principal components clearly separate the superfamilies by plastid type, and often by phyla (Fig. 2); 72% of the total variance is accounted for by the PCA. Most of the variability within the green superfamily is orthogonal to that in the red superfamily, suggesting that trace elemental profiles reflect plastid origins. Trace elemental concentrations normalized to either carbon or cell volume returned statistically similar results. A linear discriminant model<sup>12</sup> was used to classify species as either a member of the red or green plastid superfamily. Purely on the basis of elemental composition, we were

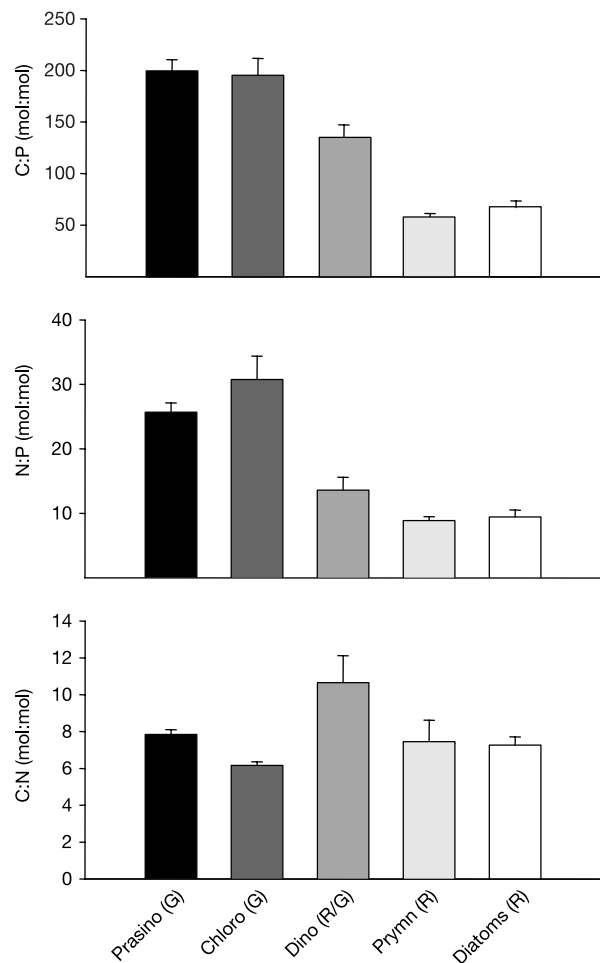


**Figure 1** C:N:P composition varies between phyla and superfamilies. Phytoplankton C:P, N:P and C:N (mol:mol) ratios are grouped phylogenetically—Prasinophyceae (Prasino) and Chlorophyceae (Chloro) are members of the green (G) plastid superfamily whereas Dinophyceae (Dino), Prymnesiophyceae (Prymn) and Bacillariophyceae (Diatoms) are members of the red (R) plastid superfamily. Error bars indicate standard errors.

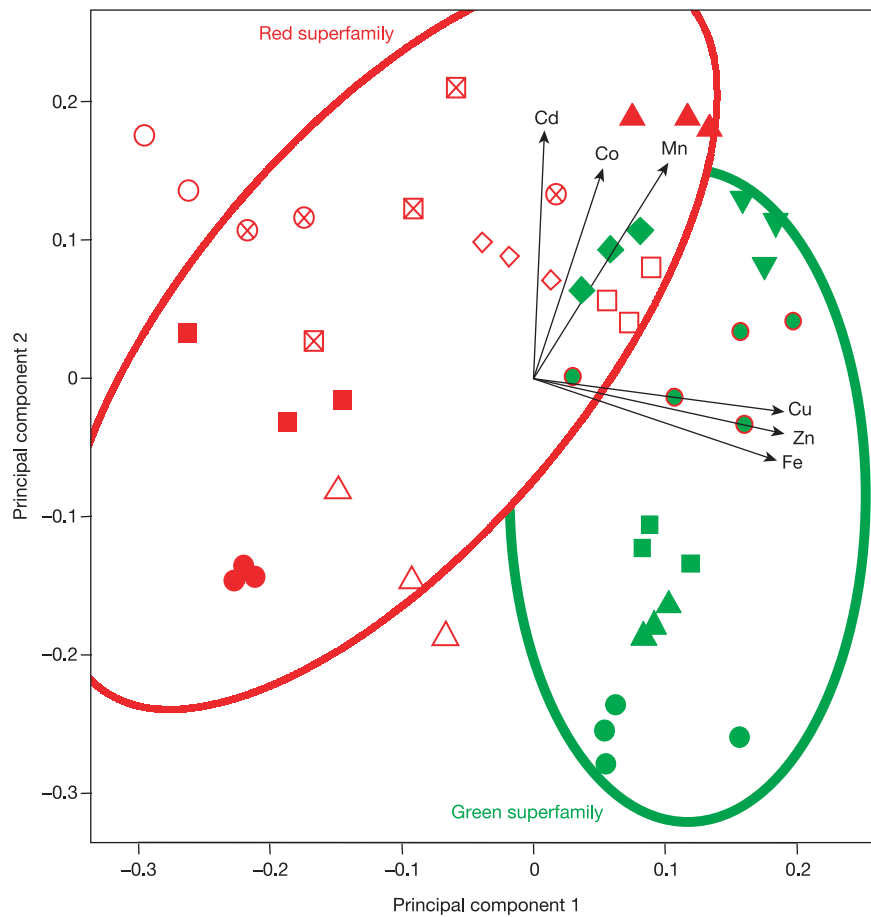


**Figure 2** Elemental profiles differentiate the green and red superfamilies. Principal component analysis of all 15 species of phytoplankton examined clusters them according to their respective superfamilies, and to a lesser degree, phyla. The principal component axes are weighted sums of the log element:P ratios (log mmol:mol P) which are shown on the figure abbreviated by the element's symbol only. The first (PC1) and second (PC2) principal components— $PC1 = 0.53 \text{ Fe} + 0.29 \text{ Mn} + 0.56 \text{ Zn} + 0.55 \text{ Cu} + 0.15$

$Co + 0.025 \text{ Cd}$ ;  $PC2 = -0.20 \text{ Fe} + 0.53 \text{ Mn} - 0.14 \text{ Zn} - 0.12 \text{ Cu} + 0.52 \text{ Co} + 0.61 \text{ Cd}$ —account for 42% and 30% of the variance respectively. Species symbols (Table 1) are centred on their location; the ellipses are used as an additional visual guide to the clustering. The length of each vector corresponds to its weighting in the first two principal components.

able to make the correct classification 85% of the time (averaged over 100 tests).

Differences in the trace elemental composition between superfamilies are the consequence of environmental selection pressures on components of the photosynthetic apparatus where metal

substitutions are possible. For example, at some point, members of the green superfamily lost their ability to express the Fe metallo-protein cytochrome  $c_6$ , and substituted plastocyanin (Cu) to ferry electrons from cytochrome  $b_6/f$  to photosystem I (ref 13). Despite this metal substitution, the Fe quotas in the green superfamily were

**Table 1** Phytoplankton phyla examined and appearance in geological record<sup>§</sup>

Geological era	Phyla	Species/clones
Proterozoic (2,500–544 Myr)	Prasinophyceae (G) (1,200 Myr)	<i>Pyramimonas parkeae</i> (CCMP 724; inverted green triangle) <i>Tetraselmis</i> sp. (CCMP 1639; green diamond) <i>Pycnococcus provasolii</i> (CCMP 1203; green square)
	Chlorophyceae (G) (1,000 Myr)	<i>Dunaliella tertiolecta</i> (CCMP 1320; green triangle) <i>Nannochloris atomus</i> (CCMP 509; green circle)
Palaeozoic (544–245 Myr)	Dinophyceae (R) (440 Myr)	<i>Gymnodinium chlorophorum</i> (DIN 3; red and green circle)* <i>Thoracosphaera heimii</i> (CCMP 1375; filled red square) <i>Prorocentrum minimum</i> (CCMP 1329; filled red triangle) <i>Amphidinium carterae</i> (CCMP 1314; filled red circle)
Mesozoic 245–65 Myr	Prymnesiophyceae (R) (210 Myr)	<i>Emiliana huxleyi</i> (ASM1; red circle and cross) <i>Gephyrocapsa oceanica</i> (JS1A; red square and cross)
	Bacillariophyceae (R) (120 Myr)	<i>Ditylum brightwellii</i> (CCMP 358; open red square) <i>Thalassiosira eccentrica</i> (CCMP 1800; open red square) <i>Thalassiosira weissflogii</i> (CCMP 1336; open red diamond) <i>Nitzschia brevirostris</i> (CCMP 551; open red triangle)

(G) and (R) indicate phyla associated with green and red plastid superfamilies respectively.

Clones were purchased from the Provasoli-Guillard National Center for Culture of Marine Phytoplankton (CCMP). *Gymnodinium chlorophorum* was obtained from the Algebank Collection (France). *Emiliana huxleyi* and *G. oceanica* were provided by I. Probert (Universite Caen Basse Normandie). Symbol descriptions in the third column are of those used in Fig. 2. Myr, million years ago.

\**Gymnodinium chlorophorum* has a chlorophyll *b*-containing (green) plastid rather than chlorophyll *c*-containing (red) plastid.

consistently higher than those for the red superfamily (Fig. 2), possibly due to higher ratios of photosystem I (containing 12 atoms of Fe) to II (containing 3 atoms of Fe) in the former<sup>14</sup>. Phytoplankton in the red superfamily typically had higher Cd and Co to P ratios (Fig. 2). The restoration of growth by Cd or Co in several species of Zn-limited diatoms and coccolithophorids may involve substitution of these elements for Zn in carbonic anhydrase<sup>15,16</sup> and perhaps other proteins. Hence, species-specific elemental profiles reflect differences in the biochemistry of the plastids.

The separation of the superfamilies in the PCA (Fig. 2) according to their plastid type does not seem to be a direct consequence of the information encoded in extant plastid genomes. An analysis of green and red plastid complete genome sequences revealed that 50 core protein-coding genes are common to all algal chloroplasts, with an additional set of 14 genes only associated with red plastids<sup>17</sup>. An examination of the mature proteins encoded in the plastid genome of extant green and red phytoplankton species reveals that they do not have significantly different trace elemental requirements. Differences in the elemental composition of the two superfamilies must therefore reflect gene transfers to the host nucleus<sup>3,4,17</sup>. The retention and expression of these genes within the nuclear genome suggests that they are essential for metabolic processes. If the key selection pressure occurred early in the evolution of the major eukaryotic phytoplankton phyla, as suggested by the phenotypic manifestation of distinct elemental profiles between plastid superfamilies, then we would predict a highly conserved set of primary and secondary gene products that are specific to the plastid type commonly inherited through nuclear genes within a superfamily.

Examining the elemental composition of extant chlorophyll *b*- and *c*-containing dinoflagellates fortuitously provides a test of this 'plastid imprint' hypothesis (Table 1; see also Supplementary Fig. 1). Assuming that the genetic backgrounds of the primordial host cells of dinoflagellates are similar, the hypothesis predicts that the trace elemental composition of dinoflagellates with plastids inherited from the red lineage would cluster more closely with other members of the chlorophyll *c*-containing superfamily, whereas dinoflagellates with green plastids would cluster with the chlorophyll *b*-containing superfamily. On the basis of trace elemental profiles, the three chlorophyll *c*-containing dinoflagellates that we examined, *Prorocentrum minimum*, *Amphidinium carterae* and *Thoracosphaera heimii*, grouped with the red superfamily, whereas the chlorophyll *b*-containing dinoflagellate, *Gymnodinium chlorophorum*, clustered with the green superfamily (Fig. 2). The host cell genetic backgrounds of all four species, however, did not discriminate among the plastid types based on C:N:P stoichiometry (Fig. 1; see also Supplementary Table 1). Our analysis indicates that the bulk elemental composition of phytoplankton is associated with the original heterotrophic host cells' genetic background and that plastid inheritance—but not the contemporary plastid genome—is a key factor determining trace elemental quotas in marine phytoplankton. Differentiation of specific trace elements by the two superfamilies further suggests that the evolutionary history of phytoplankton was strongly influenced by the redox chemistry of the ocean.

Unlike the stoichiometry of major nutrients, that of trace elements in phytoplankton does not resemble the composition of sea water (see Supplementary Fig. 2 insert). This is particularly evident of Fe and Mo, which are, respectively, the most and least abundant essential trace elements in phytoplankton, but the least and most abundant trace elements in the contemporary ocean<sup>18</sup>. Indeed, the overall pattern of the relative abundance of trace elements in the ensemble of phytoplankton examined roughly approximates that in the Earth's crust (see Supplementary Fig. 2), where Fe is abundant and Mo very scarce. A similar general trend, observed in higher plants<sup>19</sup>, suggests that there is a core elemental requirement of ancestral plastids that has been highly conserved

throughout the evolution of oxygenic photosynthesis. The high requirements for Fe and Mn and low requirement for Mo in all photoautotrophs presumably reflects the high solubility of Fe and Mn and the low solubility of Mo, Cu and other transition elements under the reducing conditions of early Proterozoic oceans<sup>20</sup>, when oxygenic photosynthesis first appeared<sup>21</sup>. This basic elemental composition helped to underpin the ecological success of the green superfamily throughout the late Proterozoic and the Palaeozoic eras. After the end-Permian extinction, and ocean anoxic events in the Triassic and Early Jurassic periods, the red superfamily rose to ecological prominence<sup>22</sup>. The relatively low Fe and Mn quotas and high Cd, Co and Mo quotas in the red superfamily suggests an adaptation of the photosynthetic apparatus and ancillary supporting proteins to a highly oxidized surface ocean, presumably in the latter half of the Phanerozoic eon<sup>22</sup>. Future studies of the trace element composition of sediments throughout the Proterozoic and Phanerozoic eons, coupled with genomic analyses of extant photoautotrophs, will almost certainly help resolve details related to the inheritance of trace element composition of phytoplankton. Our results suggest, however, that historical changes in the redox state of the ocean had a critical role in determining the evolutionary trajectory of this heterogeneous group of photosynthetic organisms. □

## Methods

### Elemental analyses

All apparatus for medium preparation, culturing, sampling and elemental analyses were prepared using trace-metal clean protocols<sup>23–25</sup>. Cultures (Table 1) were grown in a modified version of the artificial seawater medium, Aquil<sup>23</sup>, for at least six generations before sampling. We lowered the final Fe concentration to 0.36 nM and added Cd (15 nM)<sup>24</sup>. Cell numbers and sizes were measured with a calibrated Coulter multisizer particle counter to calculate growth rates and cell volumes; specific growth rates were  $\geq 90\%$  of the maximum.

Exponentially growing cultures ( $n \geq 3$ ) were collected by filtration onto precombusted Gelman AE glass fibre filters for CHN analyses and on trace-metal clean Poretics polycarbonate filters for analysis by high-resolution inductively coupled plasma mass spectrometry (HR-ICPMS). Samples for CHN analysis were dried in a desiccator at room temperature and assayed with a Carlo Erba elemental analyser. For calcifying species, a duplicate set of filters was fumed for 24 h with concentrated HCl before CHN analysis. Filtrates for HR-ICPMS were washed with either trace-metal clean synthetic ocean water<sup>23</sup> or chelexed 0.42 M NaCl<sup>24</sup>. Samples and standards for HR-ICPMS were prepared and analysed as described<sup>24,25</sup>; samples were digested in Teflon vials with 90% HNO<sub>3</sub>/10% HF at 120 °C for 4 h. Two isotopes for all elements with multi-isotopes (for example, Fe 56/57, Cu 63/65) were measured with HR-ICPMS to confirm low interference; the results for the more abundant isotope, however, were used in our analyses because of the superior counting statistics. Elemental concentrations were corrected for blanks and normalized on a per cell basis for statistical analyses.

### Statistical analyses

To determine whether the average elemental quotas were different between phyla and superfamilies, we performed a series of *t*-tests and ANOVAs with a nested design. The *P*-values for rejecting the null hypothesis (equal means in two different groups) were adjusted for multiple comparisons<sup>26</sup>. Patterns in trace elemental composition were further examined using principal component analysis<sup>12,27</sup>. The analysis was performed on Fe, Mn, Zn, Cu, Co and Cd concentrations, normalized to phosphorus and log transformed to homogenize the variances. Each species was represented as a point in six-dimensional space (one dimension for each element). The analysis was performed on the basis of correlations rather than co-variances, giving equal weight to each ratio as opposed to giving more weight to the elements with the larger ratios. The results were projected onto a plane defined by the first two principal components. Projections of a unit vector pointing along each ratio axis were calculated, making it possible to interpret how a change in position on the plot corresponded to a change in the ratio.

Received 14 April; accepted 21 July 2003; doi:10.1038/nature01953.

1. Haeckel, E. *Plankton-Studien. Vergleichende Untersuchungen über die Bedeutung und Zusammensetzung der pelagischen Fauna und Flora* (G. Fischer, Jena, 1890).
2. Delwiche, C. F. Tracing the thread of plastid diversity through the tapestry of life. *Am. Nat.* **154**, S164–S177 (1999).
3. Martin, W. *et al.* Evolutionary analysis of *Arabidopsis*, cyanobacterial, and chloroplast genomes reveals plastid phylogeny and thousands of cyanobacterial genes in the nucleus. *Proc. Natl Acad. Sci. USA* **99**, 12246–12251 (2002).
4. Palmer, J. D. The symbiotic birth and spread of plastids: how many times and howdunit? *J. Phycol.* **39**, 4–11 (2003).
5. Falkowski, P. G. & Raven, J. A. *Aquatic Photosynthesis* (Blackwell, Malden, MA, 1997).
6. Redfield, A. C. in *James Johnstone Memorial Volume* (ed. Daniel, R. J.) 176–192 (Liverpool Univ. Press, Liverpool, 1934).

7. Falkowski, P. G. Evolution of the nitrogen cycle and its influence on the biological sequestration of CO<sub>2</sub> in the ocean. *Nature* **387**, 272–275 (1997).
8. Sverdrup, H. U., Johnson, M. W. & Fleming, R. H. *The Oceans* (Prentice-Hall, New Jersey, 1942).
9. Sterner, R. W. & Elser, J. J. *Ecological Stoichiometry: The Biology of the Elements from Molecules to the Biosphere* (Princeton Univ. Press, Princeton, 2002).
10. Falkowski, P. G. Rationalizing elemental ratios in unicellular algae. *J. Phycol.* **36**, 3–6 (2000).
11. Geider, R. J. & LaRoche, J. Redfield revisited: variability of C:N:P in marine microalgae and its biochemical basis. *Eur. J. Phycol.* **37**, 1–17 (2002).
12. Venables, W. N. & Ripley, B. D. *Modern Applied Statistics with S-PLUS* (Springer, New York, 1999).
13. Raven, J. A., Evans, M. C. W. & Korb, R. E. The role of trace metals in photosynthetic electron transport in O<sub>2</sub>-evolving organisms. *Photosynth. Res.* **60**, 111–149 (1999).
14. Falkowski, P. G., Owens, T. G., Ley, A. C. & Mauzerall, D. C. Effects of growth irradiance levels on the ratio of reaction centers in two species of marine phytoplankton. *Plant Physiol.* **68**, 969–973 (1981).
15. Price, N. M. & Morel, F. M. M. Cadmium and cobalt substitution for zinc in a marine diatom. *Nature* **344**, 658–660 (1990).
16. Lee, J. G. & Morel, F. M. M. Replacement of zinc by cadmium in marine phytoplankton. *Mar. Ecol. Prog. Ser.* **127**, 305–309 (1995).
17. Grzebyk, D., Schofield, O., Vetriani, C. & Falkowski, P. G. The Mesozoic radiation of eukaryotic algae: The portable plastid hypothesis. *J. Phycol.* **39**, 259–267 (2003).
18. Whitfield, M. Interactions between phytoplankton and trace metals in the ocean. *Adv. Mar. Biol.* **41**, 3–128 (2001).
19. Williams, R. J. P. & da Silva, J. J. R. F. *The Natural Selection of the Chemical Elements* (Clarendon, Oxford, 1996).
20. Andar, A. D. & Knoll, A. H. Proterozoic ocean chemistry and the evolution: A bioinorganic bridge? *Science* **297**, 1137–1142 (2002).
21. Des Marais, D. J. When did photosynthesis emerge on Earth? *Science* **289**, 1703–1705 (2000).
22. Falkowski, P. G. et al. in *Coccolithophores: Molecular Processes to Global Impact* (eds Thierstein, H. & Young, J.) (Springer, Berlin, in the press).
23. Price, N. M. et al. Preparation and chemistry of the artificial algal culture medium Aquil. *Biol. Oceanogr.* **6**, 443–461 (1988/89).
24. Ho, T.-Y. et al. The elemental composition of some marine phytoplankton. *J. Phycol.* (submitted).
25. Cullen, J. T., Field, T. S. & Sherrell, R. M. The determination of trace elements in filtered suspended marine particulate material by sector field HR-ICP-MS. *J. Anal. At. Spectrom.* **16**, 1307–1312 (2001).
26. Benjamini, Y. & Hochberg, Y. Controlling the false discovery rate: a practical and powerful approach to multiple testing. *J. R. Stat. Soc. B* **57**, 289–300 (1995).
27. Ihaka, R. & Gentleman, R. R. Language for data analysis and graphics. *J. Comp. Graph. Stat.* **5**, 299–314 (1996).

Supplementary Information accompanies the paper on [www.nature.com/nature](http://www.nature.com/nature).

**Acknowledgements** We thank K. Wyman, C. Fuller, P. Field and R. Sherrell for assisting us with the elemental analysis, and L. Hedin, R. Sherrell and J. Raven for comments. This work was supported by the National Science Foundation 'Evolution and Radiation of Eukaryotic Phytoplankton Taxa' (EREUPT) Biocomplexity Program (Rutgers University) and the Centre for Environmental Bioinorganic Chemistry at the Princeton Environmental Institute (Princeton University).

**Competing interests statement** The authors declare that they have no competing financial interests.

**Correspondence** and requests for materials should be addressed to A.Q. ([aquigg@imcs.rutgers.edu](mailto:aquigg@imcs.rutgers.edu)) or P.G.F. ([falko@imcs.rutgers.edu](mailto:falko@imcs.rutgers.edu)).

## Predicted recurrences of mass coral mortality in the Indian Ocean

Charles R. C. Sheppard

Department of Biological Sciences, University of Warwick, Coventry CV4 7AL, UK

In 1998, more than 90% of shallow corals were killed on most Indian Ocean reefs<sup>1</sup>. High sea surface temperature (SST) was a primary cause<sup>2,3</sup>, acting directly or by interacting with other factors<sup>3–7</sup>. Mean SSTs have been forecast to rise above the 1998 values in a few decades<sup>2,3</sup>; however, forecast SSTs rarely flow seamlessly from historical data, or may show erroneous seasonal oscillations, precluding an accurate prediction of when lethal SSTs will recur. Differential acclimation by corals in different places complicates this further<sup>3,7,8</sup>. Here I scale forecast SSTs at 33

Indian Ocean sites where most shallow corals died in 1998 (ref. 1) to identify geographical patterns in the timing of probable repeat occurrences. Reefs located 10–15° south will be affected every 5 years by 2010–2025. North and south from this, dates recede in a pattern not directly related to present SSTs; paradoxically, some of the warmest sites may be affected last. Temperatures lethal to corals vary in this region by 6 °C, and acclimation of a modest 2 °C by corals could prolong their survival by nearly 100 years.

Timing of recovery from the 1998 massive coral mortality on Indian Ocean reefs (refs 1, 2, 6 and Fig. 1) and how frequently rising SSTs will cause repeat mortalities are issues of practical urgency for many countries because of the high value of reefs to shoreline protection, biodiversity, protein supply and tourism<sup>6,9,10</sup>. Raw, modelled SSTs cross supposed thresholds of coral bleaching in a few decades<sup>2</sup>, but scaling problems in forecast data, coral acclimation<sup>3,7,8</sup> and different absolute SSTs and rates of SST rise vary markedly between sites, which greatly affects estimates of when rising temperatures will reach values that proved lethal before. Exact dates remain unattainable, but a probability approach proves very revealing in terms of both timing and geographical pattern. Using the Indian Ocean, whose reefs were worst affected in the warm SSTs of 1998, I have 'blended' forecast SSTs seamlessly onto historical SST data, with appropriately scaled forecast seasonal cycles, for 33 sites.

Historical SST data from 1871–1999 from the HadISST1 data set<sup>11,12</sup> were combined with surface ('skin') temperature from 1950–2099 from the HadCM3 model for each site; the latter equates with SST (see <http://www.cru.uea.ac.uk/cru/info/modelcc/>). Both series are monthly; HadISST1 cells are 1° latitude and longitude, whereas the HadCM3 cells used are 2.5 × 3.75° (<http://www.cru.uea.ac.uk/cru/info/modelcc/>). HadISST1 comprises the latest historical data<sup>11</sup> and HadCM3 is the most recent 'coupled' model from the Hadley

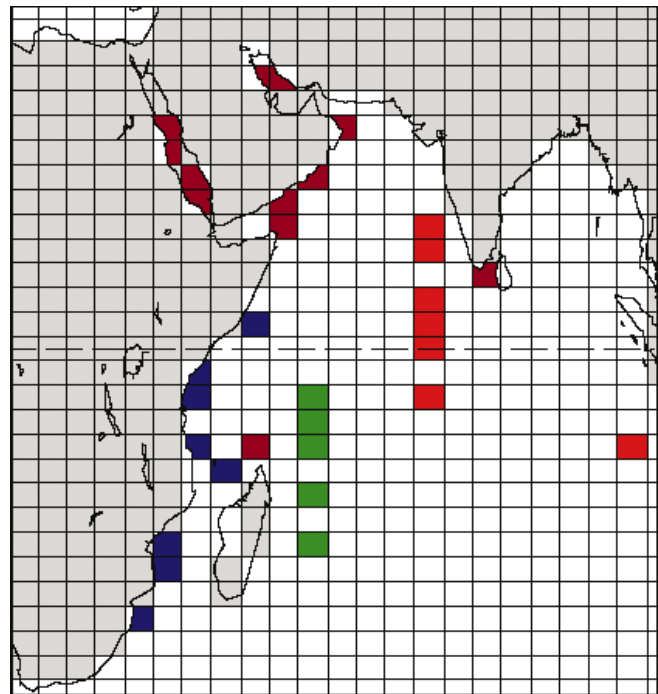


**Figure 1** Coral reef sites in the western Indian Ocean where 1998 SSTs caused mass coral mortality. The grid comprises HadCM3 cells. Blue, green and red filled cells show the transects studied; colours match the curves in Fig. 4. Brown shows additional sites examined (Arabian region, Aldabra and Sri Lanka) that do not form coherent transects (Sri Lanka is located near the central chain of atolls but is a 'high island' with reefs of very different character; Cocos Keeling, the eastern-most site, is a typical atoll and is included in the central atolls group.)